Journal of
Materials Chemistry C

ROYAL SOCIETY OF CHEMISTRY

PAPER

View Article Online
View Journal | View Issue

Check for updates

Cite this: *J. Mater. Chem. C*, 2020, **8**, 12218

Sn–N/Sn–O interaction improving electron collection in non-fullerene organic solar cells†

Lu Hu,‡[a] Nan Zhao,‡[ab] Xueshi Jiang,[a] Youyu Jiang,[a] Fei Qin,[a] Lulu Sun,[a] Wen Wang[a] and Yinhua Zhou *[a]

Received 10th January 2020,
Accepted 25th July 2020

DOI: 10.1039/d0tc00161a

rsc.li/materials-c

The electron transporting layer (ETL) is critical for achieving high performance and high stability of non-fullerene organic solar cells. However, the commonly used ZnO ETLs have the disadvantage of poor device photo-stability. Although aqueous SnO_2 can yield better stability of devices, an ''S'' shape is observed in the current density–voltage (*J*–*V*) characteristics resulting in poor device performance when it is used as an ETL in non-fullerene organic solar cells. In this paper, we have developed a method of modifying an aqueous SnO_2 solution by adding polyethylene oxide (PEO) or polyethylenimine (PEI) to eliminate the ''S'' shape characteristic of organic solar cells. PEO and PEI can interact with SnO_2 to form favorable interface dipoles and reduce the work function of the ETL films, which improves charge collection. In addition, the work function of the PEO or PEI modified SnO_2 shows better photo-stability than that of ZnO, and the devices based on the modified SnO_2 ETL also achieve higher photo-stability compared to the ZnO reference device.

Introduction

With the advantages of low cost, light weight and good mechanical flexibility, organic solar cells (OSCs) have become a competitive photovoltaic technology for the future.[1–5] In the last few years, the power conversion efficiency (PCE) of organic solar cells based on non-fullerene acceptors has exceeded 16% for single-junction cells by optimizing device structure, interface and absorber materials.[6–10] Optimizing the electron transporting layer (ETL) with high optical transmittance, a suitable energy level and high conductivity is one of the key ways to achieve high performance.[11] ZnO has become the most widely used ETL material in non-fullerene OSCs because of its easy processing and excellent photoelectric properties.[12,13] However, ZnO absorbs ultraviolet light below 380 nm and can act as a photocatalyst to decompose non-fullerene acceptors.[14] Photocatalytic activity is detrimental to the photo-stability of ZnO-based non-fullerene OSCs under illumination that contains UV light.

Recently, SnO_2 has become a very competitive ETL material owing to its high electrical conductivity, wide band gap and lower sensitivity to ultraviolet light as compared to ZnO.[15] SnO_2 has been very widely used as an ETL for high-performance perovskite solar cells.[16–18] A commercial SnO_2 aqueous colloidal dispersion (from Alfa) reported by You *et al.* can deliver high efficiency and hysteresis-free perovskite solar cells with low-temperature ($\leq$150 °C) treatment.[19,20] The SnO_2 formulation is hereafter denoted as aqueous-SnO_2. Simple processing and a low price endow it with great potential for large-scale practical applications. However, when this SnO_2 formulation is used as an ETL in non-fullerene OSCs, an ''S'' shape is observed in the current density–voltage (*J*–*V*) characteristics resulting in poor device performance (as shown by the hollow circle in Fig. 1c). This is different from another SnO_2 formulation (nanocrystal dispersion in butanol) that can deliver higher performance and better photo-stability than ZnO, as we reported previously.[14] This SnO_2 formulation is hereafter denoted as butanol–SnO_2. There is no ''S'' shape observed for the devices with butanol–SnO_2. The recipes of the two SnO_2 formulations from the vendors are not clear. We measured their work function (WF). The butanol–SnO_2 nanocrystal film shows a low WF of 4.11 eV, while the aqueous-SnO_2 shows a higher WF of 4.45 eV. This high work function is not suitable for electron collection. Starting from this point, it is expected that aqueous-SnO_2 can also work efficiently as an ETL if its work function is reduced. Polyethylenimine (PEI)[21–23] and polyethylene oxide (PEO)[24–26] are common low-WF polymer modifiers.

In this work, we reported PEO/PEI-modified SnO_2 (labeled as SnO_2–PEO/SnO_2–PEI) ETLs and their application in ternary non-fullerene organic solar cells based on PM6:Y6:IDIC.[10] The PEO and PEI modification can efficiently eliminate the ''S''

---

[a] Wuhan National Laboratory for Optoelectronics, Huazhong University of Science and Technology, Wuhan 430074, China. E-mail: yh_zhou@hust.edu.cn

[b] China-EU institute for Clean and Renewable Energy, Huazhong University of Science and Technology, Wuhan 430074, China

† Electronic supplementary information (ESI) available. See DOI: 10.1039/d0tc00161a

‡ These authors equally contributed to this work.

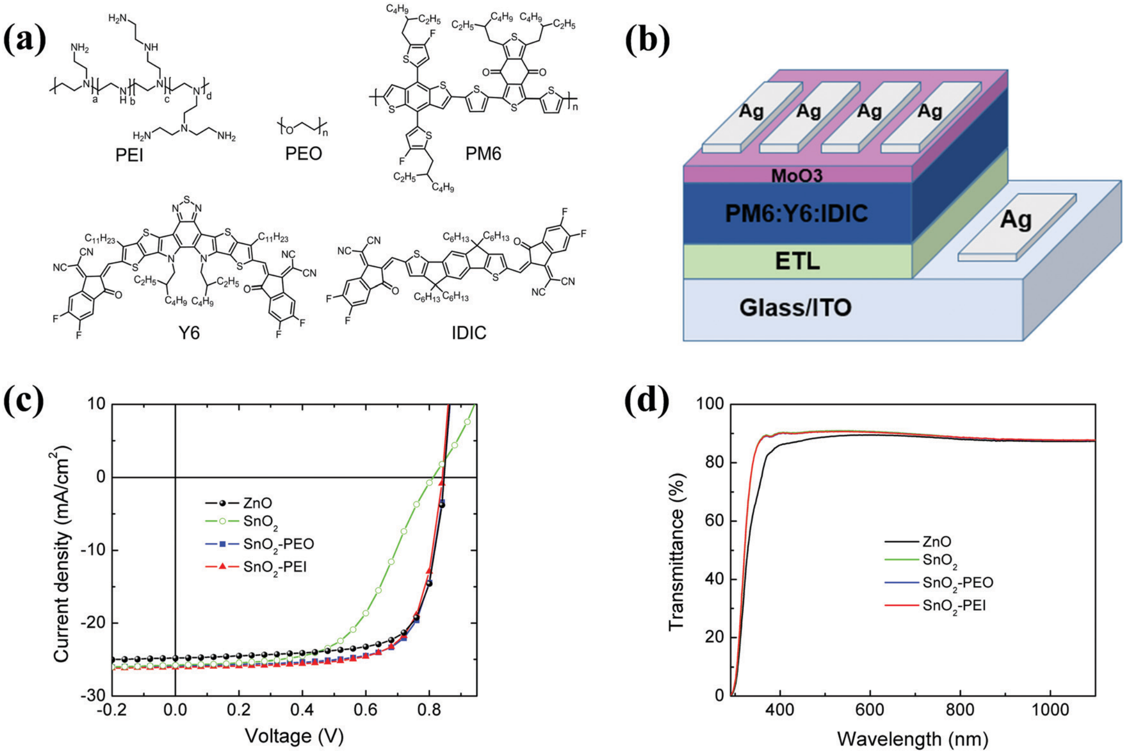

Fig. 1 (a) Chemical structure of PEI, PEO and the ternary active layer: PM6:Y6:IDIC used in this work; (b) Device structure of organic solar cells; (c) *J–V* characteristics of PM6:Y6:IDIC organic solar cells using different ETLs; (d) Transmission spectra of ETL films.

shape in the *J–V* characteristics and significantly improve the device PCE from 11.7% to 15.9% (SnO_2–PEO) and 15.8% (SnO_2–PEI). The main effect of PEO/PEI modification is associated with charge transfer and the formation of interface dipoles with SnO_2, which has been proven by X-ray photoelectron spectroscopy (XPS) and Fourier transform infrared (FTIR) spectroscopy. The modification reduces the work function of SnO_2, improving electron collection. The photo-stability of the devices with SnO_2–PEO/SnO_2–PEI is better than that of the ZnO reference device.

Experimental section

Materials

Indium tin oxide (ITO)-coated glass substrates were purchased from CSG Holding Co., Ltd. Polymer donor (PM6) and non-fullerene acceptor materials (Y6 and IDIC) were purchased from Solarmer Materials Inc. The SnO_2 colloid precursor was purchased from Alfa Aesar (tin(IV) oxide, 15% in H_2O colloidal dispersion). Before use, the SnO_2 particles were diluted with H_2O to 1.0%. PEI (99%), PEO (98%), zinc acetate dehydrates (99%), monoethanolamine (98%), chlorobenzene and 1-chloronaphthalene (CN) were purchased from Sigma-Aldrich and used as received without further purification.

Device fabrication

Non-fullerene solar cells were fabricated with an inverted configuration of ITO/ETL/active layer/MoO_3/Ag. The ITO glass substrates were cleaned stepwise with deionized water, acetone and isopropanol for 30 min. Then, the ITO substrates were treated with air plasma for 3 min. The SnO_2–PEO/SnO_2–PEI solution was prepared by dissolving PEO/PEI in the aqueous SnO_2 solution at a weight concentration of 1.5 mg mL^{-1} under stirring for 24 h. The ZnO precursor solutions were prepared by adding 0.4 g of zinc acetate dihydrate and 0.112 g of monoethanolamine into 4 mL of methoxyethanol under stirring for 12 h. The SnO_2/SnO_2–PEO/SnO_2–PEI solution was spin-coated on top of ITO glass at 3000 rpm for 30 s and then baked on a hot plate in air for 30 min at 150 °C. The ZnO precursor solution was spin-coated on top of ITO glass at 3500 rpm for 45 s followed by thermal annealing at 200 °C for 15 min in air. The PM6 : Y6 : IDIC blends with the 1 : 1 : 0.2 weight ratio were dissolved in chloroform (CF) (the concentration of the solution was 16 mg mL^{-1}) with 0.5 vol% 1-chloronaphthalene (CN). This solution was stirred at room temperature for 6 hours. The blend solution was spin-coated on top of glass/ITO/ETL at 2500 rpm for 50 s followed by thermal annealing at 90 °C for 10 min in a nitrogen (N_2)-filled glove box. Finally, MoO_3 (10 nm)/Ag electrodes (70 nm) were evaporated under a base vacuum of 1×10^{-7} Torr by using a Mini-spectros (Kurt J. Lesker) system. The effective device area was 0.041 cm^2.

Characterization

Transmittance was measured on a spectrophotometer (UV-3700, Shimadzu Scientific Instruments). *J–V* characteristics were measured under AM 1.5G irradiation (100 mW cm^{-2})

from a 450 W solar simulator (Newport 94023A-U) inside a N_2-filled glove box and recorded by a Keithley 2400 source meter. The illumination intensity was calibrated by using a silicon photodetector (Newport 818-UV). AFM images of the films were taken in tapping mode on a Shimadzu SPM9700 under ambient conditions. The XPS experiment was carried out using a Scienta ESCA 200 spectrometer. The measurements were performed in an analysis chamber at a base pressure of 10^{-10} mbar, using monochromatized Al (Kα) X-rays at $h\nu$ = 1486.6 eV. Fourier transform infrared (FTIR) spectra of the films were recorded on a Bruker VERTEX 70. Work functions of films were measured using a scanning Kelvin probe. Highly oriented pyrolytic graphite (HOPG) with a work function of 4.5 eV was used as the reference sample.

Results and discussion

Devices with an inverted structure of glass/ITO/ETL/PM6:Y6:IDIC/MoO_3/Ag were fabricated (Fig. 1b). We chose the ternary system as the active layer due to its high PCE. The structures of the materials are shown in Fig. 1a. When using SnO_2 as an ETL directly, an ''S'' shape is observed in the J–V characteristics under 100 mW cm^{-2} AM 1.5 illumination (as shown by the hollow circle in Fig. 1c). The device shows an open-circuit voltage (V_{OC}) of 0.81 V, a short-circuit current density (J_{SC}) of 25.7 mA cm^{-2}, and a fill factor (FF) of 0.56, yielding a PCE of 11.7%. Compared with the reference OSCs with ZnO as the ETL (V_{OC} = 0.85 V, J_{SC} = 25.5 mA cm^{-2}, FF = 0.72, and PCE = 15.6%), the V_{OC} of the devices is lower, and the FF is significantly reduced, which is associated with the ''S'' shape due to the poor charge collection at the interface of active layer/ETL. The cells with butanol–SnO_2 and aqueous-SnO_2 ETLs have a similar V_{OC}, but different FFs. The similar V_{OC} is possibly due to the Fermi level pinning effect. The fill factor is sensitive to the WF difference before reaching the ohmic contact at the interface.[27] To improve the performance of the devices, we added PEO or PEI (their chemical structures are shown in Fig. 1a) into the SnO_2 aqueous colloidal dispersion. The influence of PEO and PEI concentration on the WFs and the conductivities of the interlayers was studied. The work function decreases from 4.45 eV to 4.09 eV (SnO_2–PEO) and 3.99 eV (SnO_2–PEI), respectively (Fig. S1, ESI†). When the concentration of PEI and PEO increased to 1.5 mg mL^{-1}, the WF almost saturated. Thus, 1.5 mg mL^{-1} was used for the devices. When PEO and PEI were added to SnO_2, the conductivity decreased. When the concentration of PEI and PEO was 1.5 mg mL^{-1}, the conductivity was 0.011 S m^{-1} (SnO_2–PEO) and 1.75 × 10^{-3} S m^{-1} (SnO_2–PEI). After modifying SnO_2 with PEO/PEI, the ''S'' shape disappeared and a high performance was achieved: V_{OC} = 0.85 V, J_{SC} = 25.9 mA cm^{-2}, FF = 0.73 and PCE = 15.9% for PEO-modified SnO_2 (solid square in Fig. 1c), and V_{OC} = 0.84 V, J_{SC} = 26.0 mA cm^{-2}, FF = 0.72 and PCE = 15.8% for SnO_2–PEI (solid triangle in Fig. 1c). The performances are better than those of the reference OSCs with the ZnO ETL. Compared with the reference cells, the higher PCE of OSCs with the modified SnO_2 ETL arises from the enhanced J_{SC}. We can infer from Fig. 1d that the J_{SC} enhancement is due to the improved transmittance of the SnO_2 series (SnO_2, SnO_2–PEO and SnO_2–PEI) compared to ZnO.

To understand why the PEI and PEO modification improves the electron collection of aqueous-SnO_2, we first investigated the morphologies of the thin films. The atomic force microscopy (AFM) images are shown in Fig. S2 (ESI†). The root mean square (RMS) values of the roughness for the SnO_2–PEO and SnO_2–PEI samples are 2.39 nm and 2.76 nm, respectively, which are similar to that of the pristine SnO_2 (2.51 nm). In addition, the modified SnO_2 by the polymers shows reduced lateral conductivity because PEI and PEO are themselves non-conductive polymers. Even so, the conductivities are still much higher relative to that of ZnO of 2.24 × 10^{-6} S m^{-1} (Fig. S3 and Table S1, ESI†). The vertical conductivity confirms the trend (Table S1, ESI†). Based on this, the interface morphology and

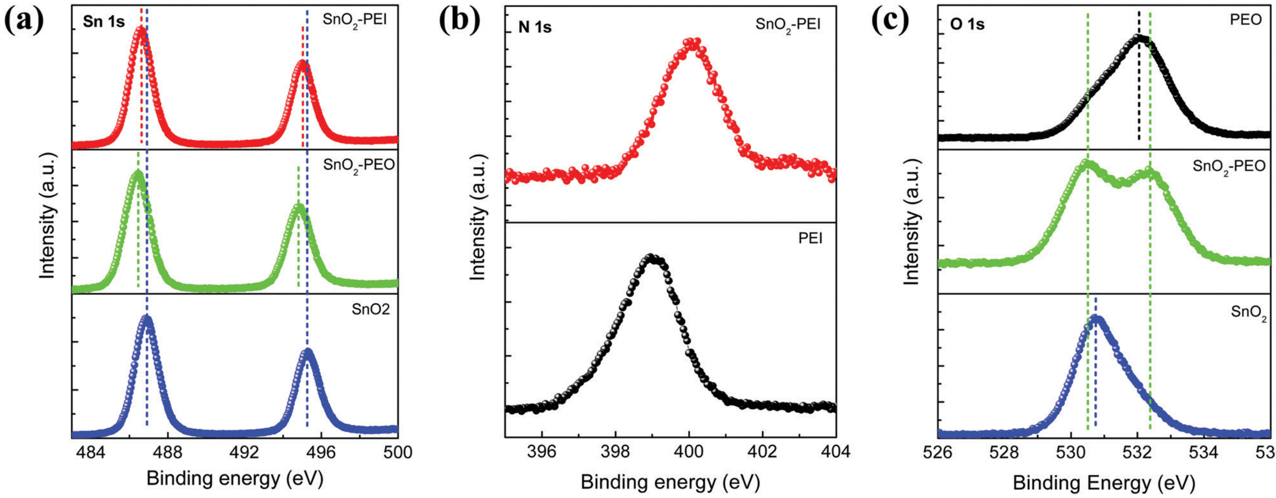

Fig. 2 (a) XPS Sn 3d core level spectra of SnO_2, SnO_2–PEI, and SnO_2–PEO films; (b) N 1s region of PEI and SnO_2–PEI films; (c) O 1s region of PEO, SnO_2 and SnO_2–PEO films.

the electrical conductivity might not be the reasons why SnO_2 modified by PEO/PEI shows improved device performance.

XPS measurement was performed to check the chemical bonding state of the SnO_2 films before and after modification. Fig. 2a presents the XPS spectra for Sn 3d of our ETL samples, while the N 1s and O 1s regions are shown in Fig. 2b and c, respectively. Fig. 2a shows that Sn $3d_{5/2}$ and Sn $3d_{3/2}$ are present in the pristine SnO_2 sample, as represented by the dominant peaks at 486.82 and 495.32 eV, respectively. Compared to SnO_2, there are slight shifts in the Sn $3d_{5/2}$ and Sn $3d_{3/2}$ binding energies at 486.43 and 494.83 eV for SnO_2–PEO and 486.57 and 495.02 eV for SnO_2–PEI, respectively. This suggests that there is interaction between PEO/PEI and SnO_2. Corresponding to the shift of Sn 3d toward a lower binding energy, Fig. 2b shows a shift in the N 1s dominant peak binding energy of SnO_2–PEI (400.03 eV) to a higher binding energy compared to that of PEI (398.95 eV). Fig. S4a and b (ESI†) show the O 1s core level spectra of SnO_2 and SnO_2–PEI. The lower binding energy XPS peak corresponds to the oxygen in the SnO_2 lattice and the higher binding energy XPS peak corresponds to the adsorbed oxygen on the surface of the films.[28,29] The percentage content of the high binding energy of the O 1s peaks of SnO_2 modified by PEI was 31.57%, which is almost the same as 34.06% before modification. Although the O 1s peaks of SnO_2–PEO are very complicated, a slight shift from 531.98 eV of PEO to 532.33 eV can still be observed due to its chemical interaction with SnO_2, as shown in Fig. 2c. Therefore, PEO and PEI interact with SnO_2. This interaction between PEI and SnO_2 is also supported by the FTIR spectra, as shown in Fig. S5 (ESI†). Compared to the pristine PEI, the characteristic absorption of $-NH_2$ stretching of SnO_2–PEI shifts toward a lower wavenumber, which is associated with a decrease of nitrogen electron cloud density. When PEI is processed from alcohol, the amine group of PEI can react with the non-fullerene acceptors.[3,30,31] Here, the PEI was processed from water. Previously, we reported that water induces the protonation of PEI and therefore suppresses the interaction between PEI and non-fullerene acceptors.[3] In addition, charge transfer from the amine in PEI to SnO_2 would further suppress the reaction (Table 1).

Fig. 3 shows the Kelvin probe measurement results of the WF for the ETL films deposited on the ITO substrates under continuous UV illumination (365 nm, 5 mW cm^{-2}) and ambient conditions. The illumination starts at 120 s and ends at 300 s (Fig. 3). The WF values are summarized in Table 2. Before illumination, the WF of SnO_2 is 4.45 eV, which is higher than 4.29 eV of ZnO. After modification by PEO or PEI, the WFs of SnO_2–PEO and SnO_2–PEI are reduced to 4.14 eV and 4.00 eV, respectively. This decrease in the WF is attributed to the formation of favorable interface dipoles by the reaction between PEO/PEI and SnO_2, which is beneficial for optimizing the energetic alignment and increasing the built-in electric field. This would be beneficial for charge collection. Therefore, the V_{OC} and FF of the devices based on the modified SnO_2 ETL show a significant enhancement. The properties of the ETL under illumination have also been studied. The WF of ZnO decreases rapidly from 4.29 eV to 3.90 eV after 3 min of illumination. In contrast, the ITO/pristine SnO_2 or modified SnO_2 films show basically no change before and after illumination. Ultraviolet illumination ($h\nu > E_g$) on ZnO will activate oxygen desorption and thus lead to reduction of the work function of the ZnO films.[32–34] The generated oxygen vacancy will result in decomposition of the non-fullerene acceptors where the blue color of the acceptors becomes bleached.[14] Both UV treatment (on ZnO) and PEO/PEI treatment (on SnO_2) can decrease the work function. But their mechanism of reducing the work function is different. UV illumination on ZnO removes oxygen and creates oxygen vacancies. Work function reduction

Table 1 Data statistics of the PM6:Y6:IDIC solar cell based on different ETLs. The device structure is glass/ITO/ETL/active layer/MoO_3/Ag

ETL	V_{OC} (V)	J_{SC} (mA cm^{-2})	FF	PCE (%)
ZnO	0.85	25.5	0.72	15.6
SnO_2	0.81	25.7	0.56	11.7
SnO_2–PEO	0.85	25.9	0.73	15.9
SnO_2–PEI	0.84	26.0	0.72	15.8

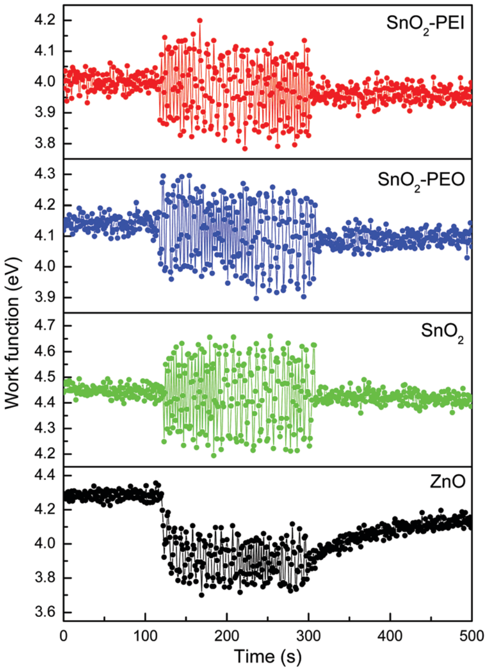

Fig. 3 Work function of ETL films under continuous UV illumination (365 nm, 5 mW cm^{-2}) in an oxygen atmosphere. The illumination starts at 120 s and ends at 300 s.

Table 2 Work functions of different ETL films extracted from the plots in Fig. 3

	$WF_{\text{Before illuminating}}$ (eV)	$WF_{\text{During illuminating}}$ (eV)	$WF_{\text{After illuminating}}$ (eV)
ZnO	4.29	3.90	4.11
SnO_2	4.45	4.44	4.42
SnO_2–PEO	4.14	4.12	4.09
SnO_2–PEI	4.00	3.98	3.96

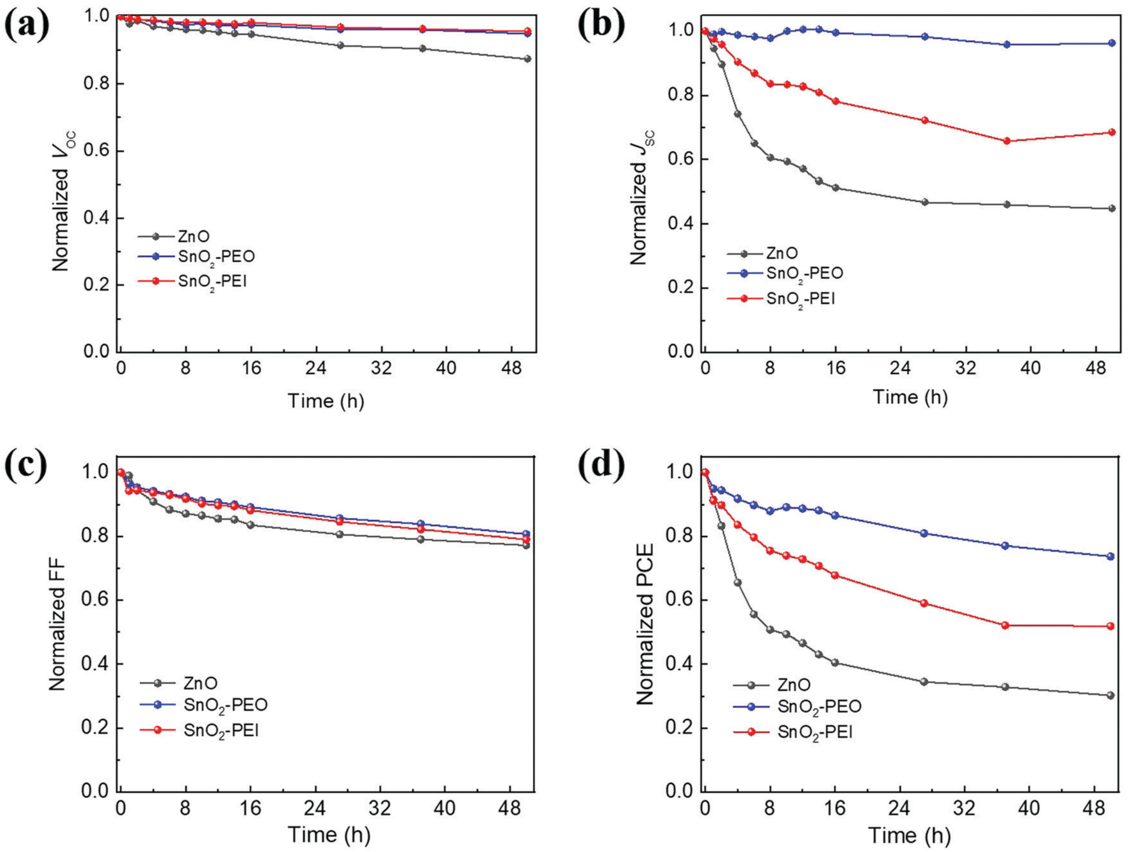

Fig. 4 Photo-stability of devices under continuous AM1.5 illumination (provided by the solar simulator) in a nitrogen-filled glove box. (a) V_{OC}, (b) J_{SC}, (c) FF, and (d) PCE.

is beneficial for electron extraction but it is detrimental to the stability of the acceptors. SnO_2 has a larger band gap of 3.4 eV that is beyond solar illumination and will not create oxygen vacancies in SnO_2 under solar illumination. The strategy of PEO/PEI modification to reduce the work function will not influence the stability of the acceptors.

Fig. 4 depicts the photo-stability of the devices under continuous AM1.5 illumination (100 mW cm^{-2}, provided by the solar simulator) for 50 h in a nitrogen-filled glove box. The original data of stability are shown in Tables S3–S6 (ESI†). After 50 h of illumination, OSCs based on ZnO show poor photo-stability and only maintain 30.2% of their initial efficiency. The device using SnO_2–PEI as the ETL retains more than half of the initial efficiency for the same test duration. When SnO_2–PEO is used as the ETL, it retains 73.7% relative to its initial efficiency even after 50 h of illumination. It is apparent that the device fabricated with the modified SnO_2 ETL shows better stability under continuous irradiation. For comparison, devices with PEI/PEO modified ZnO as ETLs were also fabricated. The devices with the PEI/PEO modified ZnO show comparable efficiency and photo-stability compared to the device with ZnO only (as shown in Fig. S7, ESI†).

Conclusions

In summary, we have demonstrated the improvement of electron collection properties of SnO_2 processed from a commercial aqueous formulation using PEO and PEI modification. Due to polymer modification, the solar cells with SnO_2–PEO and SnO_2–PEI ETLs do not show the ''S'' shape in the *J*–*V* characteristics and show a PCE of 15.9% and 15.8%, respectively, which is higher than the PCE (11.7%) of the solar cells with SnO_2 as the ETL. PEO and PEI can interact with SnO_2 to increase the interface dipoles and thus reduce the WF of SnO_2. The efficiency and FF of the devices were significantly improved. Compared with the widely used ZnO ETL, the modified SnO_2 can deliver better photo-stability. This work highlights a new perspective of high-quality ETLs obtained through modification of metal oxides by polymers.

Conflicts of interest

The authors declare no conflict of interest.

Acknowledgements

The work was supported by the National Natural Science Foundation of China (Grant No. 51773072, 51973074, and 61804060) and the Science and Technology Program of Hubei Province (2017AHB040). The authors would like to thank the Analytical and Testing Center of Huazhong University of Science and Technology for providing the facilities to conduct the characterization.

References

1 Z. He, C. Zhong, S. Su, M. Xu, H. Wu and Y. Cao, *Nat. Photonics*, 2012, **6**, 591.

2 Y. Li, G. Xu, C. Cui and Y. Li, *Adv. Energy Mater.*, 2018, **8**, 1701791.

3 S. Xiong, L. Hu, L. Hu, L. Sun, F. Qin, X. Liu, M. Fahlman and Y. Zhou, *Adv. Mater.*, 2019, **31**, 1806616.

4 L. Sun, W. Zeng, C. Xie, L. Hu, X. Dong, F. Qin, W. Wang, T. Liu, X. jiang, Y. Jiang and Y. Zhou, *Adv. Mater.*, 2020, **32**, 1907840.

5 L. Mao, B. Luo, L. Sun, S. Xiong, J. Fan, F. Qin, L. Hu, Y. Jiang, Z. Li and Y. Zhou, *Mater. Horiz.*, 2018, **5**, 123–130.

6 J. Hou, O. Inganäs, R. H. Friend and F. Gao, *Nat. Mater.*, 2018, **17**, 119.

7 C. Yan, S. Barlow, Z. Wang, H. Yan, A. K. Y. Jen, S. R. Marder and X. Zhan, *Nat. Rev. Mater.*, 2018, **3**, 18003.

8 Y. Cui, H. Yao, J. Zhang, T. Zhang, Y. Wang, L. Hong, K. Xian, B. Xu, S. Zhang, J. Peng, Z. Wei, F. Gao and J. Hou, *Nat. Commun.*, 2019, **10**, 2515.

9 B. Fan, D. Zhang, M. Li, W. Zhong, Z. Zeng, L. Ying, F. Huang and Y. Cao, *Sci. China: Chem.*, 2019, **62**, 746–752.

10 K. Li, Y. Wu, Y. Tang, M.-A. Pan, W. Ma, H. Fu, C. Zhan and J. Yao, *Adv. Energy Mater.*, 2019, **9**, 1901728.

11 D. Yang, R. Yang, K. Wang, C. Wu, X. Zhu, J. Feng, X. Ren, G. Fang, S. Priya and S. Liu, *Nat. Commun.*, 2018, **9**, 3239.

12 Y. Sun, J. H. Seo, C. J. Takacs, J. Seifter and A. J. Heeger, *Adv. Mater.*, 2011, **23**, 1679–1683.

13 R. M. Hewlett and M. A. McLachlan, *Adv. Mater.*, 2016, **28**, 3893–3921.

14 Y. Jiang, L. Sun, F. Jiang, C. Xie, L. Hu, X. Dong, F. Qin, T. Liu, L. Hu, X. Jiang and Y. Zhou, *Mater. Horiz.*, 2019, **6**, 1438–1443.

15 Q. Jiang, X. Zhang and J. You, *Small*, 2018, **14**, 1801154.

16 W. Ke, G. Fang, Q. Liu, L. Xiong, P. Qin, H. Tao, J. Wang, H. Lei, B. Li, J. Wan, G. Yang and Y. Yan, *J. Am. Chem. Soc.*, 2015, **137**, 6730–6733.

17 J. Wei, F. Guo, X. Wang, K. Xu, M. Lei, Y. Liang, Y. Zhao and D. Xu, *Adv. Mater.*, 2018, **30**, 1805153.

18 Z. Liu, K. Deng, J. Hu and L. Li, *Angew. Chem., Int. Ed.*, 2019, **131**, 11621–11628.

19 Q. Jiang, L. Zhang, H. Wang, X. Yang, J. Meng, H. Liu, Z. Yin, J. Wu, X. Zhang and J. You, *Nat. Energy*, 2016, **2**, 16177.

20 Q. Jiang, Z. Chu, P. Wang, X. Yang, H. Liu, Y. Wang, Z. Yin, J. Wu, X. Zhang and J. You, *Adv. Mater.*, 2017, **29**, 1703852.

21 Y. Zhou, C. Fuentes-Hernandez, J. Shim, J. Meyer, A. J. Giordano, H. Li, P. Winget, T. Papadopoulos, H. Cheun, J. Kim, M. Fenoll, A. Dindar, W. Haske, E. Najafabadi, T. M. Khan, H. Sojoudi, S. Barlow, S. Graham, J.-L. Brédas, S. R. Marder, A. Kahn and B. Kippelen, *Science*, 2012, **336**, 327–332.

22 C. Liu, Z. Li, X. Zhang, W. Guo, L. Zhang and S. Ruan, *ACS Photonics*, 2017, **4**, 2952–2958.

23 M. Sadeghianlemraski, B. Y. Lee, T. Davidson-Hall, Z. Leonenko and H. Aziz, *Org. Electron.*, 2019, **73**, 26–35.

24 Y. Zhou, F. Li, S. Barrau, W. Tian, O. Inganäs and F. Zhang, *Sol. Energy Mater. Sol. Cells*, 2009, **93**, 497–500.

25 S. Shao, K. Zheng, T. Pullerits and F. Zhang, *ACS Appl. Mater. Interfaces*, 2013, **5**, 380–385.

26 H. P. Dong, Y. Li, S. F. Wang, W. Z. Li, N. Li, X. D. Guo and L. D. Wang, *J. Mater. Chem. A*, 2015, **3**, 9999–10004.

27 J.-K. Tan, R.-Q. Png, C. Zhao and P. K. H. Ho, *Nat. Commun.*, 2018, **9**, 3269.

28 L. Huang, X. Sun, C. Li, J. Xu, R. Xu, Y. Du, J. Ni, H. Cai, J. Li, Z. Hu and J. Zhang, *ACS Appl. Mater. Interfaces*, 2017, **9**, 21909–21920.

29 S. Huang, N. Ali, Z. Huai, J. Ren, Y. Sun, X. Zhao, G. Fu, W. Kong and S. Yang, *Org. Electron.*, 2020, **78**, 105555.

30 X. Zhu, L. Hu, W. Wang, X. Jiang, L. Hu and Y. Zhou, *ACS Appl. Energy Mater.*, 2019, **2**, 7602–7608.

31 L. Hu, S. Xiong, W. Wang, L. Sun, F. Qin and Y. Zhou, *J. Phys. Chem. C*, 2020, **124**, 2307–2312.

32 S. Trost, T. Becker, A. Polywka, P. Görrn, M. F. Oszajca, N. A. Luechinger, D. Rogalla, M. Weidner, P. Reckers, T. Mayer and T. Riedl, *Adv. Energy Mater.*, 2016, **6**, 1600347.

33 S. Trost, A. Behrendt, T. Becker, A. Polywka, P. Görrn and T. Riedl, *Adv. Energy Mater.*, 2015, **5**, 1500277.

34 A. Manor, E. A. Katz, T. Tromholt and F. C. Krebs, *Adv. Energy Mater.*, 2011, **1**, 836–843.